ACS OMEGA

Article

Cite This: ACS Omega 2018, 3, 13636−13646

http://pubs.acs.org/journal/acsodf

# Tuning Electrochemical Bistability by Surface Area Blocking in the Cathodic Deposition of Copper

Júlia Rospendowiski,[†] Maria R. Pinto,[†] Cristian Hessel,[‡] Elton Sitta,[‡,§] and Raphael Nagao*[,†,§]

[†]Institute of Chemistry, University of Campinas, CEP 13083-970 Campinas, Sao Paulo, Brazil

[‡]Department of Chemistry, Federal University of Sao Carlos, CEP 13565-905 Sao Carlos, Sao Paulo, Brazil

[§]Center for Innovation on New Energies, University of Campinas, CEP 13083-841 Campinas, Sao Paulo, Brazil

Supporting Information

**ABSTRACT:** We report herein a precise control of the electrochemical bistability induced by surface area changes during the cathodic deposition of copper. Small additions of 1,10-phenanthroline (Phen) in the reaction media present an inhibiting effect on the global rate mainly due to the adsorption of protonated Phen. The increase of its concentration favors a shrinkage of the bifurcation (saddle-node) diagram and shifts it to less negative potentials. The dynamic instability is verified by impedance measurements, and a negative impedance is clearly found. We calculated the apparent molar mass of the adsorbents using in situ gravimetric monitoring in the electrochemical experiments, and the results indicate that mass changes occur mainly due to the reduction of copper from bivalent ions dissolved in the reaction media. Importantly, the adsorption of protonated Phen molecules does not show a considerable contribution in mass variations but prevents the formation of a copper course grained morphology over the surface. Imaging analysis indicates finer nodulations at the lower branch compared to the upper branch in the bistability domain. On the basis of these observations, a kinetic mechanism is proposed and a good agreement is obtained between the apparent molar mass extracted from experiments and the theoretical values. Altogether, our results contribute to a detailed physical chemical description of the nonlinear behavior, bringing new insights about this reaction and pointing out the possibility to design switchable surface electrodes by taking advantage of the bistable behavior.

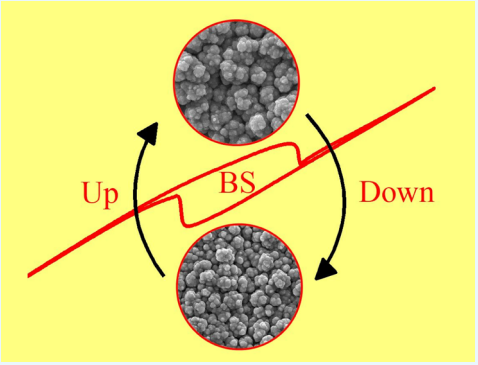




## INTRODUCTION

Nonlinear behavior in chemical systems far from equilibrium may appear in the form of dynamic instabilities.[1,2] One very frequently observed is the bistability (BS) (i.e., two stable steady states at the same set of controlling parameters), induced by a saddle-node bifurcation,[3] when positive feedback loops act as regulatory steps in the overall mechanism.[4] As a result of these self-amplifying processes, a hysteretic profile arises, and consequently, chemical switches can be designed and finely tuned by the imposition of external perturbations.[5−9] For spatially extended systems, the appearance of collective switching between states has been based on the bistable nature of the individuals,[10−13] but it can also emerge from collective behavior even if the constituents are not bistable.[14] This co-existence of different steady states has been verified in homogeneous[15−19] and heterogeneous systems.[20−22]

Electrochemical instabilities occur by the interaction of chemical properties of the solid/liquid interface (faradaic impedance) with electrical parameters of the equivalent circuit (applied voltage, current, and resistance),[23] resulting in the formation of the so-called negative differential resistance (NDR).[24] According to Koper,[25] this condition is satisfied when an increase of the double layer potential promotes a decrease of the available electrode area, the electrochemical rate constant, or the interfacial concentration of the electroactive species. Examples attending to the three cases have been reported in the literature.[26] Then, in the presence of the NDR, BS arises mainly due to the electrical autocatalysis in the electrode potential as the essential positive feedback variable [N-shaped NDR (N-NDR)][27,28] or by chemical autocatalysis stemming from a reaction intermediate [S-shaped NDR (S-NDR)].[29,30]

The emergence of BS has been observed in different electrochemical systems, such as the electroreduction of complexes of Ni(II) at a streaming mercury electrode,[31−34] in the electroreduction Hg(I)/Hg(II) ions coupled with convection,[35] in the anodic dissolution of V electrodes in acidic media,[36,37] in the electro-oxidation of small organic molecules,[38−40] and so forth. Overall, oscillations appear along with BS depending on the controlling parameters. It reveals a close correspondence between both nonlinear behaviors and corroborates with the cross-shaped phase diagram analysis.[15,16] The confirmation of the BS in these systems, under

Received: September 11, 2018
Accepted: October 1, 2018
Published: October 19, 2018




DOI: 10.1021/acsomega.8b02353
ACS Omega 2018, 3, 13636−13646

potentiostatic control, for instance, can be confirmed by impedance measurements in which zero imaginary impedance occurs in zero frequency of perturbation.[41] Although, detecting more than two branches in electrochemical systems are very rare, tristability has been observed as well.[33,42−44]

Considering the requirements to obtain a NDR, Nakanishi et al.[45] have demonstrated that additions of small amounts of 1,10-phenanthroline (Phen) in the cathodic deposition of Cu can easily induce potential and current oscillations. This study extended the previous work of Schlitter et al.[46] by a proposal of a mechanism for the electrochemical oscillations, and in short, the autocatalytic variable was recognized as the effective area of the electrode surface. To the best of our knowledge, these are the only two papers dedicated to investigate dynamic instabilities in this system. Furthermore, a more detailed study devoted to a deep understanding of the kinetics underlying the nonlinear behavior is of great interest, particularly due to the possibility to control electrochemical switches based on surface modifications.

Herein, we report the presence of BS in the electrodeposition of Cu generated by the addition of Phen in the reaction media. Two different surface deposits were observed in the same set of controlling parameters. We interpreted this type of instability mechanistically with the aid of the electrochemical quartz crystal nanobalance (EQCN), the electrochemical impedance spectroscopy (EIS), and scanning electron microscopy (SEM) images of the surface, contributing to a comprehensive physical chemical description of the nonlinear behavior. These experimental results open the possibility to design new chemical switches based on the formation of micro- or nanostructured surfaces in which the surface morphology would play an important role.

## EXPERIMENTAL SECTION

The electrochemical experiments were carried out using a counter electrode as a high area platinized-platinum foil, a reference electrode as a reversible hydrogen electrode, and a working electrode (WE) as a polycrystalline platinum sheet with an electrochemical area of 1.4 $cm^2$ inferred by the charge in the hydrogen underpotential deposition.[47,48] In case of the EQCN measurements, the WE was a disk-shaped quartz crystal 5 MHz AT cut, consisting of a Au film evaporated over a thin Ti layer—Ti/Au polished with a geometric area of 0.385 $cm^2$. Frequencies of the quartz were converted in mass variations by the Sauerbrey equation[49] with $-5.816 \times 10^{-9}$ g $Hz^{-1}$ as a constant. All glasses apparatus were cleaned by the immersion in sulfonitric solution for 12 h followed by exhaustive rinses and, at least, one boil with ultrapure water (Milli-Q Millipore, 18.2 MΩ cm).

Before each cyclic voltammetry experiment, the electrodes were cycled at 1.0 V $s^{-1}$ between 0.05 and 1.50 V for about 500 times in order to assure a reproducible surface structure. The cleanliness of the apparatus was checked from successive cyclic voltammograms at 0.05 V $s^{-1}$ until the characteristic voltammetric profile for the polycrystalline Pt electrode was observed. The supporting electrolyte was prepared by $H_2SO_4$ (Sigma-Aldrich, 95−98%) and $CuSO_4$ (Sigma-Aldrich, ≥98%) solutions using ultrapure water with final concentrations of 0.5 mol $L^{-1}$. The surface inhibition was caused by the addition of Phen (Sigma-Aldrich, ≥99%) in the reaction media.

Before the experiments, the electrolyte was kept in an ultrasonic bath for, at least, 10 min in order to obtain a better dissolution of Phen and was purged for 15 min with molecular nitrogen (White Martins, 99.99%) to remove oxygen. The electrochemical system was controlled with a potentiostat (Autolab/Eco-Chemie, PGSTAT302N) equipped with SCAN250, FRA32M, and EQCN modules. EIS was conducted at steady state with a sinusoidal potential perturbation in the frequency range of 50 kHz to 0.5 mHz and an amplitude of ±10 mV. Surface images were obtained by SEM (JEOL, JSM-6360LV), operating at 20 kV. All experiments were carried out at room temperature.

## RESULTS AND DISCUSSION

**Electrochemical Experiments.** Figure 1 depicts cyclic voltammetries at slow sweep rates of $dE/dt$ = 0.01 V $s^{-1}$ of copper sulfate in sulfuric acid solution with a final concentration of 0.5 mol $L^{-1}$ for each reagent. The potential window is 0.05−1.30 V (Figure 1a), −0.10 to 0.30 V (Figure 1b, black line), and, after the addition of 2.0 mmol $L^{-1}$ of Phen, −0.10 to 0.30 V (Figure 1b, red line). The electrodeposition of Cu is a well-known reaction studied along several decades.[50−55] As already reported in an acidic media,[52] the reduction of Cu starts around 0.30 V, following an instantaneous nucleation mechanism at very first stage of the faradaic reaction for higher concentrations of copper (e.g., 0.025 and 0.05 mol $L^{-1}$). The current density reaches −20 mA $cm^{-2}$ at 0.05 V and still shows negative values of currents up to the crossover potential of 0.30 V. From this potential, in the positive direction, it is possible to observe an intense current density peak of 32 mA $cm^{-2}$ at 0.55 V, corresponding to the oxidation of the Cu deposits and, in sequence, falling down to

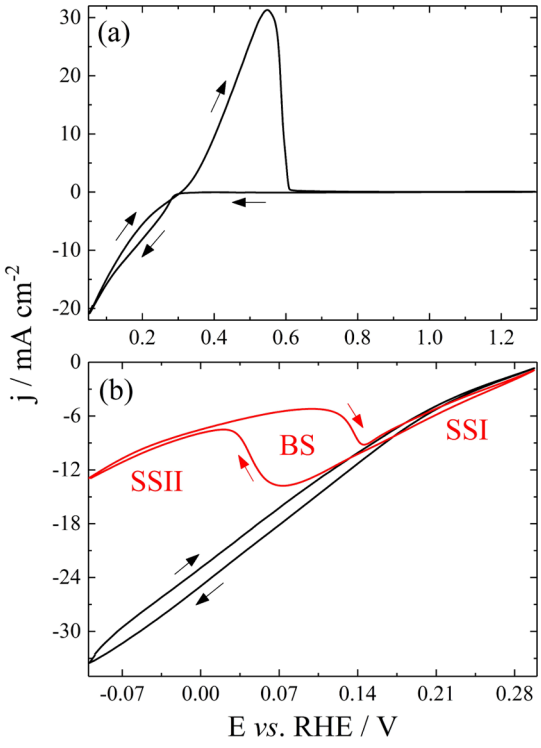


**Figure 1.** Cyclic voltammograms of the Pt|$H_2SO_4$,$CuSO_4$ system at $dE/dt$ = 0.01 V $s^{-1}$ in the potential window: (a) 0.05−1.30 and (b) −0.10 to 0.30 V (black line); same as item (b) but with addition of 2.0 mmol $L^{-1}$ of Phen (red line). SSI: steady state I; SSII: steady state II; and BS: bistability. [$H_2SO_4$] = 0.5 mol $L^{-1}$ and [$CuSO_4$] = 0.5 mol $L^{-1}$.



DOI: 10.1021/acsomega.8b02353
ACS Omega 2018, 3, 13636−13646

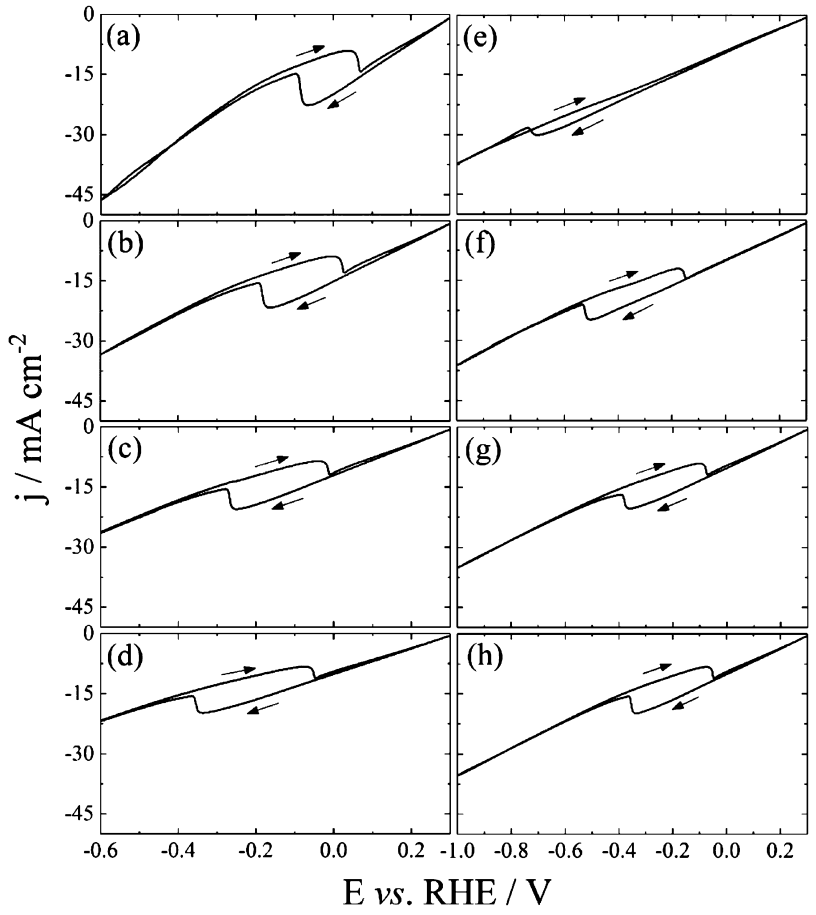


**Figure 2.** Cyclic voltammograms at $dE/dt$ = 0.01 V $s^{-1}$ under different external resistances at Phen = 2.0 mmol $L^{-1}$ and $R_{ext}$ = (a) 7, (b) 14, (c) 21, and (d) 28 Ω $cm^2$ and under the effect of the concentration of Phen at $R_{ext}$ = 28 Ω $cm^2$ and Phen = (e) 0.5, (f) 1.0, (g) 1.5, and (h) 2.0 mmol $L^{-1}$.

zero current. For $E$ > 0.62 V, Cu dissolution and a surface passivation occur.

Focusing on the potential interval of −0.10 to 0.30 V (Figure 1b), the electrodeposition of Cu takes place continuously (black line) with a small hysteresis along the positive and negative sweeps. There is a mean separation of 1.9 mA $cm^{-2}$ between the curves. However, when Phen molecules are added in the electrolyte, with a final concentration of 2.0 mmol $L^{-1}$ (red line), the deposition process is substantially suppressed for $E$ < 0.15 V. This inhibition reached a minimum value of −5.21 mA $cm^{-2}$ at 0.1 V and produced a noteworthy separation of 8.6 mA $cm^{-2}$ between the current curves along the both directions of the sweeps in the interval of 0.03−0.15 V. The suppression is more pronounced below 0.03 V, but it manifests slightly above 0.15 V as well. Nakanishi et al.[45] have postulated that adsorbed metallic complexes $[Cu(I)\text{-}(Phen)_2]^{2+}_{(ad)}$ could be mainly responsible for the inhibition and the formation of the NDR. Overall, for $E$ < 0.03 V and $E$ > 0.15 V, the hysteresis is so small that can be considered negligible. Accordingly, we considered a BS domain around the interval of 0.03 V < $E$ < 0.15 V and two steady states regions, one at $E$ > 0.15 V (SSI: steady state I) and another at $E$ < 0.03 V (SSII: steady state II).

At this point, the experimental conditions where BS can be found were, definitely, well determined. This knowledge allowed a safe variation in the controlling parameters without get too far from the BS domain. Figure 2 shows the dependence of the upper and lower potential limits of the BS by the change of the external resistance ($R_{ext}$) connected in series to the WE (Figure 2a−d) at Phen = 2.0 mmol $L^{-1}$ and the variation of concentration of Phen in the reaction media (Figure 2e−h) at $R_{ext}$ = 28 Ω $cm^2$. All mapping experiments were conducted in low sweep rates of $dE/dt$ = 0.01 V $s^{-1}$. Similar observations were done using slow rates in the cyclic voltammetries by Orlik et al.[37] Both concentration and external resistance are considered as experimentally accessible controlling parameters in electrochemical systems and can induce dynamic instabilities by subtle changes.[24]

The increase of $R_{ext}$ is followed by a progressive increase on the BS domain and it is also accompanied by a pronounced shift to negative potentials, as verified in Figure 2a−d. For external resistances of 7, 14, 21, and 28 Ω $cm^2$, the difference between the upper and lower potential limits of the BS was found to be 0.10, 0.16, 0.21, and 0.26 V, respectively (we adopted the turning points in the $j$ vs $E$ curves for the calculation). These regions do not depend on the vertex potentials in the cyclic voltammetries (Figure S1 in the Supporting Information). Indeed, the process that results in the abrupt current changes and generates the BS seems to occur in particular potentials values. This is a strong indicative that the adsorption of the inhibiting species happens in those specific potentials and remains on the surface, desorbing completely later on in the reverse cycle.

On the other hand, the increase of the concentration of Phen resulted in a shrinkage of the BS domain. At the lowest employed concentration of Phen, that is, 0.5 mmol $L^{-1}$, only



DOI: 10.1021/acsomega.8b02353
ACS Omega 2018, 3, 13636−13646

the lower limit is observed and an expressive hysteretic profile does not arise (Figure 2e). When the concentration of Phen is increased to 1.0 mmol $L^{-1}$ a different scenario appears and the BS is clearly established under these conditions (Figure 2f). Note that the approximation of the upper and lower limits to an invariable potential became even more evident in larger concentrations of Phen, that is, 1.5 or 2.0 mmol $L^{-1}$ (Figure 2g–h). No significant changes were observed in these two concentrations, which indicate a surface saturation of the inhibiting species above of 1.5 mmol $L^{-1}$.

A summary of the effect of $R_{ext}$ and concentration of Phen on the bistable behavior in the electrodeposition of Cu is shown in terms of a bifurcation diagram in Figure 3. At first

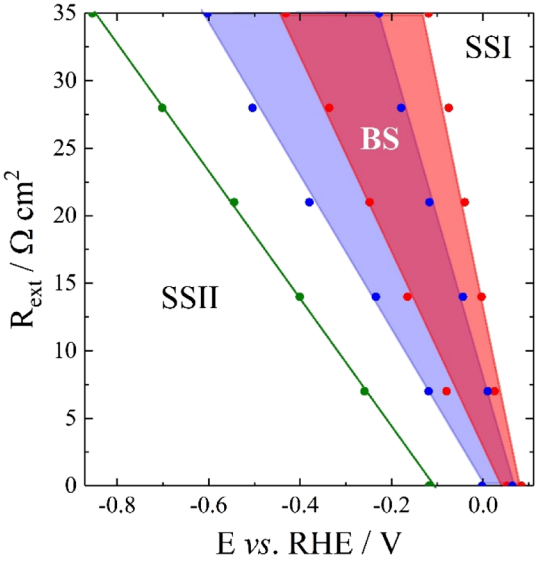


**Figure 3.** Bifurcation diagram $R_{ext}$ vs $E$ measured at sweep rate of $dE/dt$ = 0.01 V $s^{-1}$ in several concentrations of Phen: 0.5 mmol $L^{-1}$ (green line), 1.0 mmol $L^{-1}$ (blue line), and 2.0 mmol $L^{-1}$ (red line). SSI: steady state I; SSII: steady state II; and BS: bistability.

glance, its shape has a considerable resemblance with the bifurcation diagrams of systems belonging to an N-NDR category.[26] In fact, Nakanishi et al.[45] have observed electrochemical oscillations in both current and potential, which is a good indicative that the cathodic deposition of Cu perturbed with Phen remains in the hidden N-NDR (HN-NDR) subsystem. H means that the NDR can be partially hidden from an intermediate that blocks the surface and reduces the global rate in lower potentials.[23,24]

Additionally, Figure 3 highlights the saddle-node bifurcation[3] as the lines surrounding the domains of the BS and how it is strongly modified by the increase of the concentration of Phen. A straight green line represents the slight suppression of the current when [Phen] = 0.5 mmol $L^{-1}$ is added into the electrolyte. The contraction of the BS domains reaches a maximum around 1.5 mmol $L^{-1}$, and negligible changes are observed when compared to the domain formed at 2.0 mmol $L^{-1}$ (Figures 2g,h and S2 in the Supporting Information). The calculated areas of these diagrams are 7.9 and 6.3 V Ω $cm^2$ for 1.0 and 2.0 mmol $L^{-1}$ of Phen, respectively. This compression in the bifurcation diagram by inhibiting species is in agreement with the numerical simulations performed by Nascimento et al.[56] A considerable shrinkage of the Hopf domain was observed as the irreversible surface poisoning evolved. The dynamics changed accordingly and the chaotic oscillations were dramatically suppressed.

The saddle-node bifurcation can be confirmed by the EIS under potentiostatic control when the imaginary part of the impedance is zero as the frequency of perturbation tends to zero as well,[41] that is, $Z'(\omega) = 0$ for $\omega = 0$. Figure 4 depicts

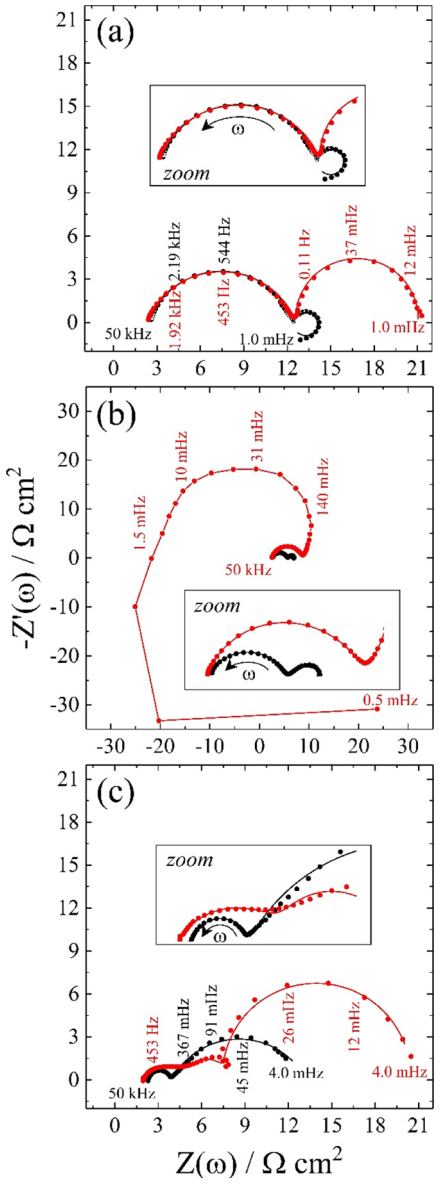


**Figure 4.** Nyquist plots for the electroreduction of Cu without (black lines) and with (red lines) Phen molecules in the concentration of 2.0 mmol $L^{-1}$ at the applied voltages: (a) $E$ = 0.24 V, (b) $E$ = 0.12 V, and (c) $E$ = −0.05 V. The insets correspond to a "zoom in" on the plates (a–c). Sinusoidal amplitude of perturbation is ±10 mV from 50 kHz to 0.5 mHz.

Nyquist plots of the electrodeposition of Cu in three different applied voltages of 0.24, 0.12, and −0.05 V which are located at the SSI, the BS domain, and the SSII, respectively. Black lines indicate the cathodic reduction of Cu without the presence of Phen, whereas in red lines, Phen is present in the reaction media. We modeled the frequency responses by equivalent circuits for the impedances shown in Figure 4a,c



DOI: 10.1021/acsomega.8b02353
*ACS Omega* 2018, 3, 13636–13646

and extracted the respective electrical parameters (Figure S3 and Table S1 in the Supporting Information).

Figure 4a shows that the process has distinct time scales with the presence of two semicircles, one at higher and another at lower frequencies. They are related to two limiting steps which compete simultaneously and are affected by the applied voltage—high frequencies describe activation control, whereas low frequencies describe mass transport control.[57] In the latter, the Warburg impedance shows a decreasing imaginary component, resulting in the observed trend[58] (Figure 4a, black line). It has been also ascribed that low-frequency loops are strongly dependent of the growth mode of copper deposits.[59,60] There are different interpretations for the inductive behavior in the lowest frequencies, but it can represent the adsorption−desorption of inhibiting species, for example, anions from the electrolyte[61] or a nucleation process[59,60] (Figure 4a, black line). The Ohmic drop ($R_\Omega$) shows very low values of around 2.2 Ω cm$^2$ in all experiments.

Interestingly, the first semicircle is not affected by the presence of the Phen but causes a significant increase in the real and imaginary components of the low-frequency loop (Figure 4a, red line). As the dominant loop belongs to the higher frequency spectrum, the global faradaic reaction is not highly affected by the Phen molecules under the voltage of 0.24 V. Figure 1b reflects that this description where no significant suppression is observed and similar charge transfer resistances ($R_{ct}$) of 10 Ω cm$^2$, with and without the presence of Phen, corroborates with this scenario. Nevertheless, there is a slight increase in the constant phase element from 21.4 to 29.9 $\mu$F cm$^{-2}$. For the second process located in lower frequencies, the polarization resistance increases from 2.1 to 8.4 Ω cm$^2$, reflecting the surface inhibiting effect of the Phen (Figure 4a, red line).

The dynamic instability induced by Phen becomes even clearer in the Figure 4b. The first observation is the anticlockwise movement in lower frequencies on the Nyquist plot and the subsequent intersection in the real axis at 1.5 mHz which is related to the Hopf bifurcation, that is, $Z'(\omega) = 0$ for $\omega \neq 0$ (Figure 4b, red line). In fact, the hidden negative impedance [$Z'(\omega) < 0$ for $\omega \neq 0$] suggests that the system belongs to the HN-NDR class[41] and consequently confirms the proposition already discussed.[45] Accordingly, the autocatalytic evolution of the double layer potential is driven by surface area changes, which makes a very easy handling of the BS domain by the control of the concentration of Phen.

Figure 4c depicts an expressive decrease of the diameter of the high-frequency loop because of the fast charge transfer of the copper ions on the surface. Indeed, the lowest resistance of $R_{ct}$ = 1.62 Ω cm$^2$ is observed for this process (Figure 4c, black line) and larger faradaic rates are in agreement with it (Figure 1b, black line). As also expected, a mass transport limitation acts in this applied voltage and bigger semicircles can be observed in lower frequencies.[61] However, we believe that the presence of Phen has a strong effect on the Cu deposits growth and the low-frequency loop is mainly attributed to the inhibition of the surface by the adsorption of metallic complexes (Figure 4c, red line), having Phen as ligands, which induces the decrease of the overall current (Figure 1b, red line). The imaginary components showed an evident capacitive effect of 390−687 mF cm$^{-2}$ when Phen is added into the reaction media.

**Gravimetric Monitoring.** In this section, we will provide further insights on the nature of the adsorbed species and it will allow us to propose a mechanistic interpretation of how BS appears in this system. Figure 5 shows the $j$ vs $E$ curves

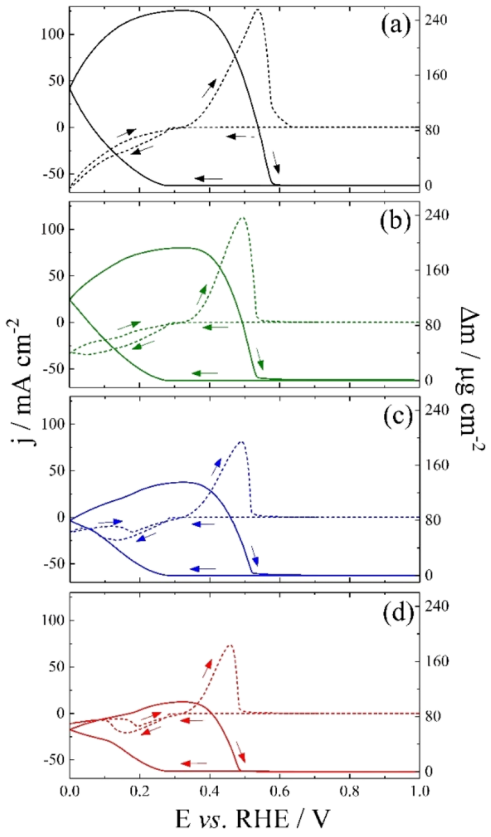


**Figure 5.** Current densities (dashed line) and mass variations (full line) at d$E$/d$t$ = 0.02 V s$^{-1}$ with additions of Phen as final concentrations of (a) 0 (black), (b) 0.5 mmol L$^{-1}$ (green), (c) 1.0 mmol L$^{-1}$ (blue), and (d) 2.0 mmol L$^{-1}$ (red). [$H_2SO_4$] = 0.5 mol L$^{-1}$ and [$CuSO_4$] = 0.5 mol L$^{-1}$.

(dashed line) during the electroreduction of Cu at d$E$/d$t$ = 0.02 V s$^{-1}$ followed by the corresponding mass changes profiles (full lines) obtained with the aid of the EQCN. The system was perturbed with small additions of Phen as final concentrations of 0 (black), 0.5 mmol L$^{-1}$ (green), 1.0 mmol L$^{-1}$ (blue), and 2.0 mmol L$^{-1}$ (red). To study the BS domains by mass variation measurements ($\Delta m$), the limit potentials were set at 0−1.0 V in order to prevent the continuous accumulation of Cu on the surface by its dissolution in higher potentials and, then, preventing a monotonic ascending curve of $\Delta m$. For this reason, the mass changes profiles were normalized to zero at $E$ = 1.0 V.

As observed in Figure 5 the crossover potential is 0.3 V but a significant deposition of Cu occurs only for $E$ < 0.26 V and begins to decay around $E$ > 0.35 V in the positive direction. The removal of deposited Cu is dependent on the concentration of Phen. As it increases, the suppression of the global rate can be evidenced by the decrease of the oxidative and reductive currents followed by the reduction of the corresponding mass changes profiles in the positive and negative sweeps, respectively. Interestingly, an expressive variation of the mass can be observed in the lower and upper potential limits of the BS domains, where the curve $\Delta m$ vs $E$ flips the concavity and bends, forming a considerable angle especially at higher concentrations of Phen. This



DOI: 10.1021/acsomega.8b02353
ACS Omega 2018, 3, 13636−13646

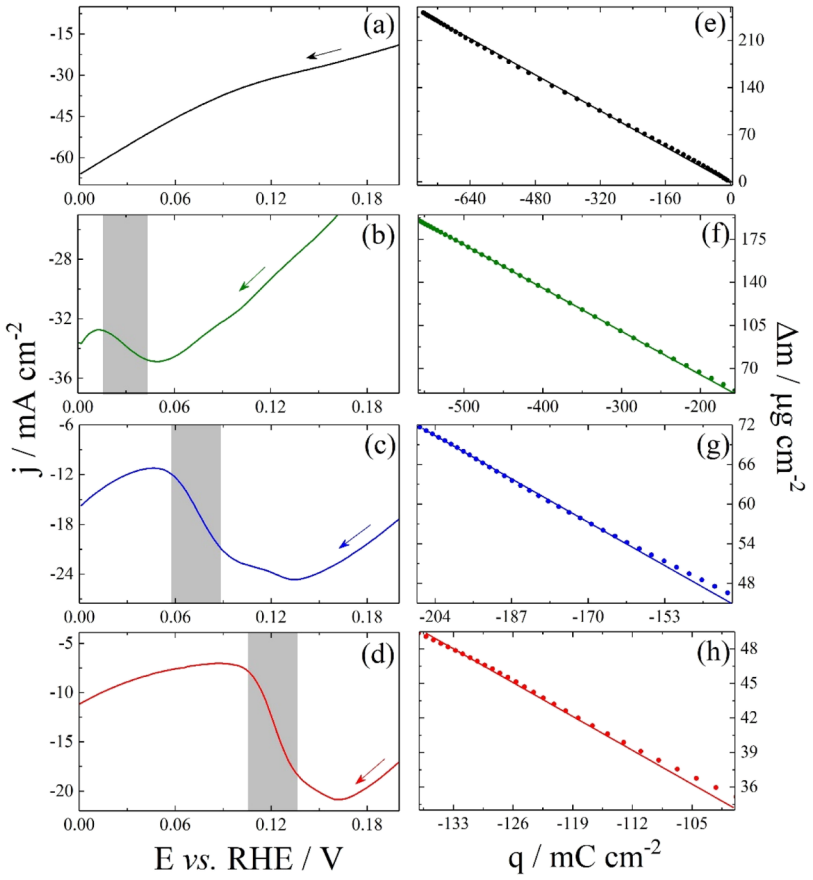


**Figure 6.** (a–d) $j$ vs $E$ and (e–h) $\Delta m$ vs $q$ in the potential interval of 0–0.20 V. The arrows indicate the direction of the sweep. The curves follow the color code used in the text for Phen concentrations: 0 (black), 0.5 mmol $L^{-1}$ (green), 1.0 mmol $L^{-1}$ (blue), and 2.0 mmol $L^{-1}$ (red). The gray bands represent the potential window, where mass/charge ratios were calculated.

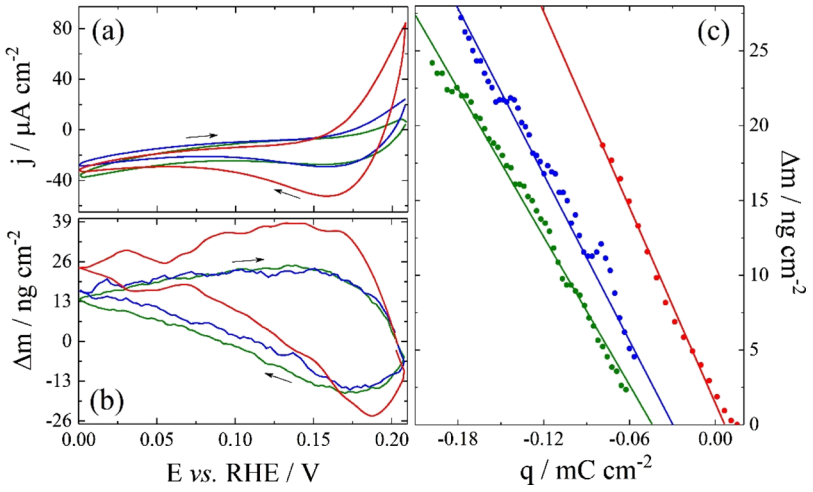


**Figure 7.** (a) $j$ vs $E$, (b) $\Delta m$ vs $E$, and (c) $\Delta m$ vs $q$ in the potential interval of 0–0.20 V in the absence of copper sulfate. The curves follow the color code used as previously: 0.5 mmol $L^{-1}$ (green), 1.0 mmol $L^{-1}$ (blue), and 2.0 mmol $L^{-1}$ (red). $[H_2SO_4]$ = 0.5 mol $L^{-1}$.

observation suggests that there is a strong adsorption of species dissolved in the electrolyte during the negative sweep. This abrupt current suppression is detailed in Figure 6. When it is turned to positive direction, the adsorbed species are released from the surface and the Cu deposition occurs quicker.

Focusing on the potential interval of 0–0.20 V, it was possible to calculate the mass/charge ($m/z$) ratios from $j$ vs $E$ and $\Delta m$ vs $E$ curves in the negative sweep as represented by the arrows. The colors assignments are the same of the Figure 5. The experimental $m/z$ ratio for the electrodeposition of Cu without the presence of Phen (Figure 6a,e) is 332 $\mu$g $C^{-1}$, which agrees with the theoretical value of 329 $\mu$g $C^{-1}$ and retracts the electroreduction of $Cu^{2+}$ to $Cu^0$ on the surface. In this calculation, we used the molar mass of 63.5 g $mol^{-1}$ for Cu and 2 electrons for the faradaic reaction, that is, 63.5 g $mol^{-1}$/2 × 96 485 C $mol^{-1}$. As long as the Phen concentration



DOI: 10.1021/acsomega.8b02353
ACS Omega 2018, 3, 13636–13646

increases, the $m/z$ values increases as well. In this respect, we can safely consider that the process attributed to the adsorption, responsible to generate the instability in the negative sweep, takes place more intensely following the ascending order: [Phen] = 0.5 mmol $L^{-1}$ and 352 $\mu$g $C^{-1}$ (Figure 6b,f), [Phen] = 1.0 mmol $L^{-1}$ and 392 $\mu$g $C^{-1}$ (Figure 6c,g), and [Phen] = 2.0 mmol $L^{-1}$ and 416 $\mu$g $C^{-1}$ (Figure 6d,h). The effect of adsorption of protonated Phen was studied separately, vide Figure 7.

Nakanishi et al.[45] have postulated that the reduced form of the adsorbed metallic complexes $[Cu(I)(Phen)_2]^{2+}_{(ad)}$ could be the responsible for the inhibition effect, but it was observed mainly in neutral media.[62] In acidic environment, the ligands could be totally protonated, which would weaken the coordination bonds between $Cu^{2+}$ and Phen and, therefore, generate uncoordinated ligands molecules. According to this description, Phen might also participate in the adsorption process causing the inhibition effect simultaneously with the adsorption of the metallic complexes.[63] Figure 7a depicts cyclic voltammograms of the system Cu|$H_2SO_4$,Phen under different concentrations of Phen. In this potential region, there is no Cu dissolution (Figure S4 in the Supporting Information) and the anodic and cathodic currents can be associated with desorption and adsorption processes, respectively. Large currents are observed in higher concentrations of Phen.

Figure 7b shows that the respective mass profiles corroborate with the processes discussed previously. Note, however, that the mass scale is now in nanograms. In the positive sweep, the mass variations decrease for $E > 0.17$ V and increase in the negative sweep starting at $E < 0.19$ V. In this respect, one can conclude that in NDR region observed during copper electrodeposition, the Phen molecules (or their protonated form) interact with the surface competing for adsorption sites. We have tried to explain the nature of Phen adsorbate by $m/z$ ratios in the potential interval of 0.07−0.15 V, cf. Figure 7c. Straight lines with a good fit were obtained and correspond to 166 $\mu$g $C^{-1}$ (green line), 170 $\mu$g $C^{-1}$ (blue line), and 181 $\mu$g $C^{-1}$ (red line).

As observed, these values do not show big discrepancies between each other and are approximately 10 times lower than those expected to the Phen adsorption in a one-electron process, thus suggesting unknown charge transfer processes occurring simultaneously at this potential window (Figure S4 in the Supporting Information). In certain extension, the adsorption of protonated Phen can be considered a fast equilibrium with the dissolved molecules in the interface, which modifies the total coverage of the adsorbed species and ends up with underestimated values of $m/z$. In the next sections, we will provide a more realistic information, or physical sense, by converting $m/z$ ratios in apparent molar mass and, finally, propose a kinetic mechanism to the emergence of the BS.

**Imaging Analysis.** Corroborating with the previous measurements, this section will support the overall discussion by extracting surface images with the aid of the SEM. Nakanishi et al.[45] have inspected the electrodeposit surface and observed two types of surface morphologies during the electrochemical oscillations: leaflet-like particles of a few micrometers in size and dense round-shaped leaflets, which are associated with low and high current states, respectively. Cu leaflets would occur in an anisotropic crystal growth by a selective adsorption on a specific crystalline facet inhibiting the global reaction. Interestingly, in a bistable state, the addition of Phen resulted in a completely different morphology, reflecting the emergence of structured surfaces driven by distinct dynamic instabilities.

Figure 8 depicts SEM images of the surface at three applied voltages: 0.24 V (SSI), 0.12 V [bistability, upper ($BS_u$) and lower ($BS_d$) branches, and −0.05 V (SSII)]. For each experiment, we cycled 20 times between −0.1 and 0.3 V at $dE/dt = 0.01$ V $s^{-1}$, pulled out the WE in the desired voltage and sequentially disconnected it from the potentiostat. This procedure assured a good reproducibility. The images show that the surface morphology of the electroplated deposit depends on the applied voltage and the presence of Phen in the reaction media. Regarding the SSI, in the potential region, where Phen alters slightly the current density (Figure 1b), a fine globular structure is clearly seen. As the potential slowly decreases, this fine structure moves toward a roundish nodule morphology, vide $BS_d$. Then, after the abrupt suppression of the current by the adsorption of reaction intermediates, the system reaches a state where massive deposition of Cu takes place.

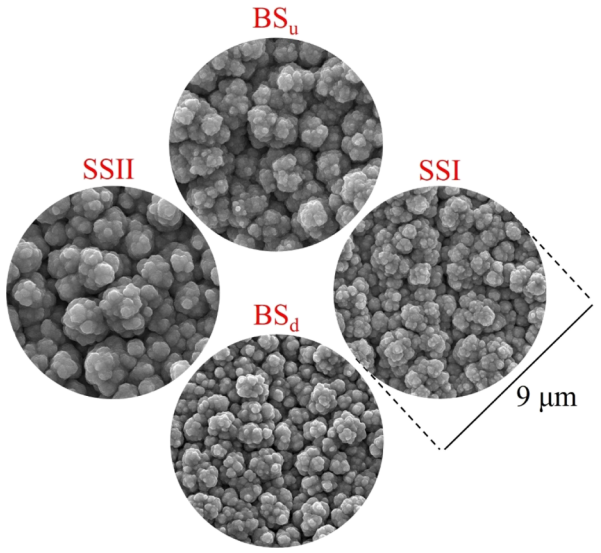


**Figure 8.** Electronic micrographs of the electrode surface after the electrodeposition of Cu perturbed with 2.0 mmol $L^{-1}$ of Phen. The samples were obtained at the potentials of 0.24 V (SSI), 0.12 V ($BS_u$ and $BS_d$ as the upper and lower branches of the BS domain, respectively), and −0.05 V (SSII). The diameter of the images is 9 $\mu$m.

The image taken in the SSII represents this situation and evidences the production of thick Cu films, which are coarse-grained and uniform along the electrode. Similar observations have been reported in the electrodeposition of copper.[64,65] Finally, in the reverse scan, the surface structure gradually changes to a finer globular formation again as seen in $BS_u$. However, this return is not totally completed to the SSI state and visual differences are observed in the images found at $BS_u$ and $BS_d$. Overall, the $BS_u$ surface structure has a lower number of fine nodulations and embranchments compared to $BS_d$. The system is very sensitive to the initial conditions and, for this reason, exhibits a memory effect. In fact, this characteristic is a strong evidence of the presence of BS. According to the surface inhibition provoked by the addition of Phen, these molecules seem to prevent the formation of coarse grained structures


DOI: 10.1021/acsomega.8b02353
ACS Omega 2018, 3, 13636−13646

because it demonstrates a substantial inhibiting effect in the reaction of Cu deposition.

**Mechanistic Interpretation.** The initial voltammetric characterization presented in Figure 1 attests the inhibition effect of the Phen in the electrodeposition of Cu. In fact, it has been proposed that metallic complexes have a strong adsorption on the surface, which reduce the total active area.[45] Phen molecules have also a favorable interaction with metallic surfaces[66−69] and can easily change its orientation depending on the applied voltage.[70,71] Therefore, not only the metallic complexes could induce dynamic instabilities but also the ligands by a significant adsorption process. Herein, we provide mechanistic information about the effect of the blocking species using a combination of surface techniques.

First, it is important to consider that the reaction media, where the study was conducted, is highly acidic with $[H_2SO_4]$ = 0.5 mol $L^{-1}$ and $[CuSO_4]$ = 0.5 mol $L^{-1}$ or pH → 0. As the $pK_a$ of the $[H(Phen)]^+$ and $[H(Phen)_2]^+$ species are 5.12 and 2.11, respectively,[72−74] the Phen molecules are protonated in the nitrogen atoms. Hence, for $pK_a$ > pH, it is expected to observe the following reactions in the bulk of the solution

$$Phen_{(aq)} + H^+_{(aq)} \rightleftharpoons [H(Phen)]^+_{(aq)} \quad (r1)$$

$$[H(Phen)]^+_{(aq)} + Phen_{(aq)} \rightleftharpoons [H(Phen)_2]^+_{(aq)} \quad (r2)$$

For the sake of simplicity, we neglected the contribution of the $[H(Phen)_2]^+_{(aq)}$ species in the analysis, although it has been also detected experimentally in a self-stacking mechanism.[75,76] Because copper sulfate is also added into the electrochemical cell

$$Cu^{2+}_{(aq)} + 2[H(Phen)]^+_{(aq)} \rightleftharpoons [Cu(II)(Phen)_2]^{2+}_{(aq)} + 2H^+_{(aq)} \quad (r3)$$

which shows an oxidized form of the metallic complex as the dominant species in the solution. It is proposed that it can adsorb on the surface and compete in parallel with the deposition of Cu.

The electrochemical reduction of Cu in the solid/liquid interface takes place as

$$Cu^{2+}_{(aq)} + 2e^- \rightarrow Cu^0 \quad (r4)$$

This reaction proceeds through two steps, and the rate determinant step is considered to be the first electron reception by the bivalent ion.[77] We write this reaction in a short form r4. On the other hand, the electrons transfer in the metallic complex happens in an adsorption pathway[45]

$$[Cu(II)(Phen)_2]^{2+}_{(aq)} + e^- + * \rightleftharpoons [Cu(I)(Phen)_2]^+_{(ad)} \quad (r5)$$

in our electrochemical mechanism, asterisk means free active sites on the surface. The nature of the adsorbed complex is still not clear but experimental evidences in different substrates, concentrations, and solution pH have shown to be $[Cu(I)(Phen)_2]^+_{(ad)}$.[78−80] Nevertheless, in very strong acidic media as ours, the protonation of the nitrogen in the Phen molecules is energetically favorable. Because of the positively charged reactants, the formation of the coordinated bonds is not easily performed and a complex dissociation would occur as well. Naturally, the formation of the NDR is severely dependent on the pH, being its appearance facilitated when pH increases.[45]

This reaction intermediate has a short-lived state, and it is rapidly reduced to metallic Cu in lower potentials[78,79]

$$[Cu(I)(Phen)_2]^+_{(ad)} + e^- \rightarrow Cu^0 + 2Phen_{(aq)} + * \quad (r6)$$

Then, larger concentrations of Phen result in steeper slopes $j$ vs $E$ during the inhibition process and a shift to less negative potentials. As the dynamic equilibrium of the reaction r5 has an impact on the total coverage of the adsorbed metallic complexes, the mass variations would be associate mainly with the electrochemical deposition of Cu (the reduction evolving a metallic complex should shift the onset potential, but it is not verified in our experiments). Although the concentration of Phen is much lower than $Cu^{2+}_{(aq)}$, a fast equilibrium might be observed by those remaining protonated molecules which are not coordinated with Cu

$$[H(Phen)]^+_{(aq)} + e^- + * \rightleftharpoons Phen_{(ad)} + H^+_{(aq)} \quad (r7)$$

We can now use the $m/z$ ratios and convert them to apparent molar mass ($M_{app}$), considering the faradaic process. Figure 6 provides the following information in each concentration of Phen: 352 $\mu$g $C^{-1}$ (0.5 mmol $L^{-1}$), 392 $\mu$g $C^{-1}$ (1.0 mmol $L^{-1}$), 416 $\mu$g $C^{-1}$ (2.0 mmol $L^{-1}$). We already know the electroreduction of $Cu^{2+}$ has a theoretical value of 329 $\mu$g $C^{-1}$, and hence, the experimentally measured $m/z$ ratios represent mostly the reaction r4. This observation is in agreement with the large difference between the concentrations of copper sulfate and Phen in the reaction media and the massive electrochemical deposition of Cu during the gravimetric measurements. In this respect, the faradaic reactions r5−r7 participate only with 23 $\mu$g $C^{-1}$ (0.5 mmol $L^{-1}$), 63 $\mu$g $C^{-1}$ (1.0 mmol $L^{-1}$), and 87 $\mu$g $C^{-1}$ (2.0 mmol $L^{-1}$) because of the discount of 329 $\mu$g $C^{-1}$ from the total value.

These $m/z$ ratios are quite small, and if the conversion is made for a 1 electron transfer reaction, they can be associated with $M_{app}$: 2.2, 6.1, and 8.4 g $mol^{-1}$, respectively. The results point out that none of the metallic complex intermediates, containing Cu (63.5 g $mol^{-1}$) or Phen (180.2 g $mol^{-1}$), could be adsorbed on the surface because of their high molar mass. Note that our model does not take in to account the participation of water molecules and (bi)sulfate anions dissolved in the electrolyte, and possibly, those small changes could be also related to it. Performing the calculation using the derivative $d\Delta m/dC$ vs $E$ along 0−0.2 V (Figure S5 in the Supporting Information), it is possible to obtain point-by-point the $m/z$ ratios. Clearly, the reaction r4 is dominant and takes place over the total interval of 0−0.2 V, and the $m/z$ ratios slightly diverge from 329 $\mu$g $C^{-1}$ in the abrupt current suppressions shown in Figure 6.

On the basis of these experimental results, we can conclude that the adsorbed intermediates do not alter mass variations significantly during the formation of the NDR but can inhibit the reduction of copper ions and modify drastically the global faradaic reaction as observed in Figures 1 and 5. It was found that Phen molecules are adsorbed vertically on Cu(111) with their nitrogen atoms facing the substrate.[71] The molecules were stacked to form polymer-like chains because of the $\pi$-electron attraction in the aromatic ring among them. The adlayer of Phen formed on Cu surface changes depending on the applied voltage and it is considered more organized in positive potentials. If the electrolyte is kept in acidic conditions, the molecular plane of Phen is inclined toward



DOI: 10.1021/acsomega.8b02353
ACS Omega 2018, 3, 13636−13646

the metal surface,[66] which could further enhance the inhibition factor.

Our experimental results converge to the idea that the inhibiting effect of the global faradaic reaction could be related with the adsorption of Phen—the protonated Phen molecules coordinate with $Cu^{2+}$ in a negligible extension because of the highly acidic media (two positively charged reactants). Then, reactions r5 and r6 should not be present and the equilibrium in the reaction r3 is definitely shifted to the left. Additionally, the adsorption of protonated Phen on the Cu surface might occur in a fast equilibrium with the molecules on the interface, impacting on the total coverage of the adsorbed species and resulting in underestimated values of $m/z$, vide Figures 6 and 7. It might be also considered a weak adsorption driven possibly by physical interactions, which does not contribute to meaningful mass variations, but still affects the Faradaic reaction of the electrochemical reduction of Cu.

## CONCLUSIONS

We have studied the effect of Phen in the electrochemical reduction of Cu under strong acidic media by means of different surface techniques. Overall, Phen molecules are found to be protonated and the coordination with copper ions dissolved in the solution seems to be unfavorable. The Phen molecules adsorb on the surface and inhibit the reduction of $Cu^{2+}$ from the solution. This blocking process alters significantly the area of the electrode and induces an autocatalytic evolution of the double layer potential. As experimentally observed, this dynamic behavior promotes the formation of a bistable domain, delineated by a saddle-node bifurcation, in a wide range of controlling parameters, such as the external resistance, the applied voltage, and the concentration of Phen.

The increase of the concentration of Phen favors a shrinkage of the bifurcation diagram and shifts it to less negative potentials. Besides voltammetric characterization, the EIS measurements also converge to a conclusion of an inhibiting process. The instability generated by adsorption was confirmed by the hidden negative impedance, that is, $Z'(\omega) < 0$ for $\omega \neq 0$, indicating a HN-NDR system. The EQCN experiments show that the mass variations take place mainly by the electrodeposition of Cu from the bivalent ions, and consequently, the adsorption of dissolved Phen molecules does not show an important contribution in this respect.

A kinetic mechanism is proposed based on the observations, and a good agreement is obtained between the apparent molar mass extracted from experiments and the theoretical values. Surface images indicate that Phen prevents the formation of coarse grained structures and the BS domain is composed by two different surface morphologies—the lower branch has finer nodulations compared to the upper branch. Finally, we believe that our results can trigger the design of a switchable surface electrodes taking advantage from the easy access to a bistable behavior. A reversible change in the coverage of the Phen could turn "on" or "off" two different surface states multiple times.

## ASSOCIATED CONTENT

### Supporting Information

The Supporting Information is available free of charge on the ACS Publications website at DOI: 10.1021/acsomega.8b02353.

Cyclic voltammetries; bifurcation diagram $R_{ext}$ vs $E$; equivalent circuits for the EIS measurements; electrical parameters extracted by mathematical modeling of the impedance analysis; and $\Delta m$ versus $E$ and $d\Delta m/dC$ vs $E$ plots (PDF)

## AUTHOR INFORMATION


### Corresponding Author

*E-mail: nagao@iqm.unicamp.br.

### ORCID

Elton Sitta: 0000-0003-3181-0076

Raphael Nagao: 0000-0001-8400-9093


### Notes

The authors declare no competing financial interest.

## ACKNOWLEDGMENTS

J.R. (17/11835-7), M.R.P. (17/05592-4), and R.N. (16/22262-5) acknowledge São Paulo State Foundation (FAPESP), and C.H. acknowledges Coordination for the Improvement of Higher Education Personnel (CAPES) for the scholarships. R.N. (16/01817-9) and E.S. (13/07296-2) acknowledge FAPESP for financial support. The authors acknowledge Camilla Abbehausen for fruitful discussions about coordination chemistry and Cleo Pires for the assistance to obtain the preliminary SEM images.

## REFERENCES


(1) Scott, S. K. *Oscillations, Waves, and Chaos in Chemical Kinetics*; Oxford University Press: Oxford, 1994.

(2) Epstein, I. R.; Pojman, J. A. *Introduction to Nonlinear Chemical Dynamics: Oscillations, Waves, Patterns and Chaos*; Oxford University Press: New York, 1998.

(3) Strogatz, S. H. *Nonlinear Dynamics and Chaos: With Applications to Physics, Biology, Chemistry, and Engineering*; Addison-Wesley: Cambridge, 1994.

(4) Wilhelm, T. The Smallest Chemical Reaction System with Bistability. *BMC Syst. Biol.* **2009**, *3*, 90.

(5) Silverberg, J. L.; Na, J.-H.; Evans, A. A.; Liu, B.; Hull, T. C.; Santangelo, C. D.; Lang, R. J.; Hayward, R. C.; Cohen, I. Origami Structures with a Critical Transition to Bistability Arising from Hidden Degrees of Freedom. *Nat. Mater.* **2015**, *14*, 389−393.

(6) Sato, O. Dynamic Molecular Crystals with Switchable Physical Properties. *Nat. Chem.* **2016**, *8*, 644−656.

(7) Hagiwara, H.; Masuda, T.; Ohno, T.; Suzuki, M.; Udagawa, T.; Murai, K.-i. Neutral Molecular Iron(II) Complexes Showing Tunable Bistability at Above, Below, and Just Room Temperature by a Crystal Engineering Approach: Ligand Mobility into a Three-Dimensional Flexible Supramolecular Network. *Cryst. Growth Des.* **2017**, *17*, 6006−6019.

(8) Wu, D.-Q.; Shao, D.; Wei, X.-Q.; Shen, F.-X.; Shi, L.; Kempe, D.; Zhang, Y.-Z.; Dunbar, K. R.; Wang, X.-Y. Reversible On-Off Switching of a Single-Molecule Magnet via a Crystal-to-Crystal Chemical Transformation. *J. Am. Chem. Soc.* **2017**, *139*, 11714−11717.

(9) Amirjalayer, S.; Martinez-Cuezva, A.; Berna, J.; Woutersen, S.; Buma, W. J. Photoinduced Pedalo-Type Motion in an Azodicarboxamide-Based Molecular Switch. *Angew. Chem., Int. Ed.* **2018**, *57*, 1792−1796.

(10) Kouvaris, N. E.; Kori, H.; Mikhailov, A. S. Traveling and Pinned Fronts in Bistable Reaction-Diffusion Systems on Networks. *PLoS One* **2012**, *7*, No. e45029.

(11) Crespo-Yapur, D. A.; Bonnefont, A.; Schuster, R.; Krischer, K.; Savinova, E. R. Sequential Activation and Oscillations of Globally Coupled Microelectrodes during a Bistable Reaction. *ChemElectroChem* **2014**, *1*, 1046−1056.




DOI: 10.1021/acsomega.8b02353
*ACS Omega* 2018, 3, 13636−13646

(12) Kouvaris, N. E.; Sebek, M.; Mikhailov, A. S.; Kiss, I. Z. Self-Organized Stationary Patterns in Networks of Bistable Chemical Reactions. *Angew. Chem., Int. Ed.* **2016**, *55*, 13267−13270.
(13) Bozdech, S.; Biecher, Y.; Savinova, E. R.; Schuster, R.; Krischer, K.; Bonnefont, A. Oscillations in an Array of Bistable Microelectrodes Coupled through a Globally Conserved Quantity. *Chaos* **2018**, *28*, 045113.
(14) Gogia, G.; Burton, J. C. Emergent Bistability and Switching in a Nonequilibrium Crystal. *Phys. Rev. Lett.* **2017**, *119*, 178004.
(15) Boissonade, J.; De Kepper, P. Transitions from bistability to limit cycle oscillations. Theoretical analysis and experimental evidence in an open chemical system. *J. Phys. Chem.* **1980**, *84*, 501−506.
(16) De Kepper, P.; Boissonade, J. Theoretical and experimental analysis of phase diagrams and related dynamical properties in the Belousov-Zhabotinskii system. *J. Chem. Phys.* **1981**, *75*, 189−195.
(17) Ouyang, Q.; Noszticzius, Z.; Swinney, H. L. Spatial bistability of two-dimensional Turing patterns in a reaction-diffusion system. *J. Phys. Chem.* **1992**, *96*, 6773−6776.
(18) Kaminaga, A.; Vanag, V. K.; Epstein, I. R. A Reaction-Diffusion Memory Device. *Angew. Chem., Int. Ed.* **2006**, *45*, 3087−3089.
(19) Szalai, I.; De Kepper, P. Turing Patterns, Spatial Bistability, and Front Instabilities in a Reaction-Diffusion System. *J. Phys. Chem. A* **2004**, *108*, 5315−5321.
(20) Bär, M.; Nettesheim, S.; Rotermund, H. H.; Eiswirth, M.; Ertl, G. Transition between Fronts and Spiral Waves in a Bistable Surface Reaction. *Phys. Rev. Lett.* **1995**, *74*, 1246−1249.
(21) Bodega, P. S.; Alonso, S.; Rotermund, H. H. Effects of External Global Noise on the Catalytic CO Oxidation on Pt(110). *J. Chem. Phys.* **2009**, *130*, 084704.
(22) De Decker, Y.; Baras, F. Bistability and Explosive Transients in Surface Reactions: The Role of Fluctuations and Spatial Correlations. *Eur. Phys. J. B* **2010**, *78*, 173−186.
(23) Krischer, K.; Varela, H. Oscillations and Other Dynamic Instabilities. In *Handbook of Fuel Cells: Fundamentals, Technology and Applications*; Vielstich, W., Lamm, A., Gasteiger, H. A., Eds.; John Wiley & Sons: Chichester, 2003; Vol. *2*, pp 679−701.
(24) Krischer, K. Nonlinear Dynamics in Electrochemical Systems. In *Advances in Electrochemical Science and Engineering*; Alkire, R. C., Kolb, D. M., Eds.; Wiley-VCH: Weinheim, 2003; Vol. *8*, pp 90−203.
(25) Koper, M. T. M. The Theory of Electrochemical Instabilities. *Electrochim. Acta* **1992**, *37*, 1771−1778.
(26) Orlik, M. Self-Organization in Electrochemical Systems I: General Principles of Self-Organization. *Temporal Instabilities*; Springer-Verlag: Berlin Heidelberg, 2012.
(27) Mukouyama, Y.; Kawasaki, H.; Hara, D.; Yamada, Y.; Nakanishi, S. Appearance of New Oscillations (Named Oscillations I and J) during Reduction of $H_2O_2$ on Platinum Electrode. *J. Electrochem. Soc.* **2017**, *164*, H1−H10.
(28) Mukouyama, Y.; Kawasaki, H.; Hara, D.; Yamada, Y.; Nakanishi, S. Appearance of New Oscillation (Named Oscillation H) Induced by $Na_2SO_4$ and $K_2SO_4$ in Electroreduction of $H_2O_2$ on Platinum. *J. Electrochem. Soc.* **2017**, *164*, H675−H684.
(29) Siegmeier, J.; Baba, N.; Krischer, K. Bistability and Oscillations during Electrooxidation of $H_2$-CO Mixtures on Pt: Modeling and Bifurcation Analysis. *J. Phys. Chem. C* **2007**, *111*, 13481−13489.
(30) Bozdech, S.; Krischer, K.; Crespo-Yapur, D. A.; Savinova, E.; Bonnefont, A. 1/f(2) noise in bistable Electrocatalytic Reactions on Mesoscale Electrodes. *Faraday Discuss.* **2016**, *193*, 187−205.
(31) Jurczakowski, R.; Orlik, M. Bistable/Oscillatory System Based on the Electroreduction of Thiocyanate Complexes of Nickel(II) at a Streaming Mercury Electrode. Experiment and Simulation. *J. Phys. Chem. B* **2002**, *106*, 1058−1065.
(32) Orlik, M.; Jurczakowski, R. On the Stability of Nonequilibrium Steady-States for the Electrode Processes at a Streaming Mercury Electrode. *J. Phys. Chem. B* **2002**, *106*, 7527−7536.
(33) Jurczakowski, R.; Orlik, M. Experimental and Theoretical Studies of the Multistability in the Electroreduction of the Nickel(II)−$N_3$−Complexes at a Streaming Mercury Electrode. *J. Phys. Chem. B* **2003**, *107*, 10148−10158.
(34) Jurczakowski, R.; Orlik, M. Experimental and Theoretical Impedance Studies of Oscillations and Bistability in the Ni(II)-SCN Electroreduction at the Streaming Mercury Electrode. *J. Electroanal. Chem.* **2007**, *605*, 41−52.
(35) Gorzkowski, M. T.; Jurczakowski, R.; Orlik, M. Electrochemical Oscillations and Bistability in the Redox Processes of Mercury Ions, Coupled with the Self-Induced Convection of Hg Surface. *J. Electroanal. Chem.* **2008**, *615*, 135−144.
(36) Gorzkowski, M. T.; Orlik, M. Electrochemical Oscillations and Bistability during Anodic Dissolution of Vanadium Electrode in Acidic Media-Part II. The model. *J. Solid State Electrochem.* **2011**, *15*, 2321−2330.
(37) Gorzkowski, M. T.; Wesołowska, A.; Jurczakowski, R.; Ślepski, P.; Darowicki, K.; Orlik, M. Electrochemical oscillations and bistability during anodic dissolution of vanadium electrode in acidic media-part I. Experiment. *J. Solid State Electrochem.* **2011**, *15*, 2311−2320.
(38) Xu, Y.; Schell, M. Bistability and Oscillations in the Electrocatalyzed Oxidation of Formaldehyde. *J. Phys. Chem.* **1990**, *94*, 7137−7143.
(39) Cai, X.; Schell, M. Observation of Bistability in Cyclic Voltammetric Experiments on Ethanol, Propanol, Butanol and Formic Acid/Formate. *Electrochim. Acta* **1992**, *37*, 673−680.
(40) Chen, S.; Schell, M. Bistability and Excitability in the Electrochemical Oxidation of Ethanol. *Electrochim. Acta* **1999**, *44*, 4773−4780.
(41) Strasser, P.; Eiswirth, M.; Koper, M. T. M. Mechanistic classification of electrochemical oscillators - an operational experimental strategy. *J. Electroanal. Chem.* **1999**, *478*, 50−66.
(42) Schell, M. Mechanistic and Fuel-Cell Implications of a Tristable Response in the Electrochemical Oxidation of Methanol. *J. Electroanal. Chem.* **1998**, *457*, 221−228.
(43) Chen, S.; Schell, M. A Comparison of Multistability in the Electrocatalyzed Oxidations of Methanol and Ethanol in Acid and Alkaline Solutions. *J. Electroanal. Chem.* **1999**, *478*, 108−117.
(44) Chen, S.; Schell, M. Excitability and Multistability in the Electrochemical Oxidation of Primary Alcohols. *Electrochim. Acta* **2000**, *45*, 3069−3080.
(45) Nakanishi, S.; Sakai, S.-i.; Nishimura, K.; Nakato, Y. Layer-by-Layer Electrodeposition of Copper in the Presence of o-Phenanthroline, Caused by a New Type of Hidden NDR Oscillation with the Effective Electrode Surface Area as the Key Variable. *J. Phys. Chem. B* **2005**, *109*, 18846−18851.
(46) Schlitter, F. W.; Eichkorn, G.; Fischer, H. Rhythmisch lamellares kristallwachstum bei der elektrolytischen kupferabscheidung. *Electrochim. Acta* **1968**, *13*, 2063−2075.
(47) Trasatti, S.; Petrii, O. A. Real Surface Area Measurements in Electrochemistry. *Pure Appl. Chem.* **1991**, *63*, 711−734.
(48) Lukaszewski, M.; Soszko, M.; Czerwinski, A. Electrochemical Methods of Real Surface Area Determination of Noble Metal Electrodes - An Overview. *Int. J. Electrochem. Sci.* **2016**, *11*, 4442−4469.
(49) Bandey, H. L.; Martin, S. J.; Cernosek, R. W.; Hillman, A. R. Modeling the Responses of Thickness-Shear Mode Resonators under Various Loading Conditions. *Anal. Chem.* **1999**, *71*, 2205−2214.
(50) Bockris, J. O.; Conway, B. E. Determination of the Faradaic Impedance at Solid Electrodes and The Electrodeposition of Copper. *J. Chem. Phys.* **1958**, *28*, 707−716.
(51) Gunawardena, G.; Hills, G.; Montenegro, I. Electrochemical nucleation. *J. Electroanal. Chem.* **1985**, *184*, 357−369.
(52) Grujicic, D.; Pesic, B. Electrodeposition of Copper: The Nucleation Mechanisms. *Electrochim. Acta* **2002**, *47*, 2901−2912.
(53) Grujicic, D.; Pesic, B. Reaction and Nucleation Mechanisms of Copper Electrodeposition from Ammoniacal Solutions on Vitreous Carbon. *Electrochim. Acta* **2005**, *50*, 4426−4443.
(54) Radisic, A.; Ross, F. M.; Searson, P. C. In Situ Study of the Growth Kinetics of Individual Island Electrodeposition of Copper. *J. Phys. Chem. B* **2006**, *110*, 7862−7868.


DOI: 10.1021/acsomega.8b02353
*ACS Omega* 2018, 3, 13636−13646

(55) Abbott, A. P.; El Ttaib, K.; Frisch, G.; McKenzie, K. J.; Ryder, K. S. Electrodeposition of Copper Composites from Deep Eutectic Solvents Based on Choline Chloride. *Phys. Chem. Chem. Phys.* **2009**, *11*, 4269−4277.
(56) Nascimento, M. A.; Nagao, R.; Eiswirth, M.; Varela, H. Coupled Slow and Fast Surface Dynamics in an Electrocatalytic Oscillator: Model and Simulations. *J. Chem. Phys.* **2014**, *141*, 234701.
(57) Burke, L. D.; Sharna, R. AC Impedance Investigation of Copper in Acid Solution. *J. Electrochem. Soc.* **2008**, *155*, D285−D90.
(58) Shao, W.; Pattanaik, G.; Zangari, G. Electrochemical Nucleation and Growth of Copper from Acidic Sulfate Electrolytes on n-Si(001). *J. Electrochem. Soc.* **2007**, *154*, D339−D207.
(59) Chassaing, E.; Wiart, R. Epitaxial Growth and Electrode Impedance of Copper Electrodeposits. *Electrochim. Acta* **1984**, *29*, 649−660.
(60) Wiart, R. Elementary steps of electrodeposition analysed by means of impedance spectroscopy. *Electrochim. Acta* **1990**, *35*, 1587−1593.
(61) Gabrielli, C.; Moçotéguy, P.; Perrot, H.; Wiart, R. Mechanism of Copper Deposition in a Sulphate Bath Containing Chlorides. *J. Electroanal. Chem.* **2004**, *572*, 367−375.
(62) Lee, C. W.; Anson, F. C. Electron Exchange Between $Cu(Phen)_2^+$ Adsorbed on Graphite and $Cu(Phen)_2^{2+}$ in Solution. *Inorg. Chem.* **1984**, *23*, 837−844.
(63) Doe, H.; Yoshioka, K.; Kitagawa, T. Voltammetric Study of Protonated 1,10-Phenanthroline Cation Transfer Across the Water/Nitrobenzene Interface. *J. Electroanal. Chem.* **1992**, *324*, 69−78.
(64) Schmidt, W. U.; Alkire, R. C.; Gewirth, A. A. Mechanic Study of Copper Deposition onto Gold Surfaces by Scaling and Spectral Analysis of In Situ Atomic Force Microscopic Images. *J. Electrochem. Soc.* **1996**, *143*, 3122−3132.
(65) Nichols, R. J.; Beckmann, W.; Meyer, H.; Batina, N.; Kolb, D. M. An In Situ Scanning Tunnelling Microscopy Study of Bulk Copper Deposition and the Influence of an Organic Additive. *J. Electroanal. Chem.* **1992**, *330*, 381−394.
(66) Zawada, K.; Bukowska, J. An interaction of 1,10-phenantroline with the copper electrode in neutral and acidic aqueous solutions: a surface enhanced Raman scattering study. *J. Mol. Struct.* **2000**, *555*, 425−432.
(67) Muniz-Miranda, M.; Pergolese, B.; Bigotto, A. SERS and DFT Investigation on the Adsorption of 1,10-Phenanthroline on Transition Metal Surfaces. *Phys. Chem. Chem. Phys.* **2010**, *12*, 1145−1151.
(68) Andrade, G. F. S.; Temperini, M. L. A. 1,10-Phenanthroline Adsorption on Iron Electrode Monitored by Surface-Enhanced Raman Scattering (SERS). Comparison to SERS of Phen and Its Transition Metal Complex on Silver Electrode. *J. Phys. Chem. C* **2007**, *111*, 13821−13830.
(69) Peng, Y.; Niu, Z.; Huang, W.; Chen, S.; Li, Z. Surface-Enhanced Raman Scattering Studies of 1,10-Phenanthroline Adsorption and its Surface Complexes on a Gold Electrode. *J. Phys. Chem. B* **2005**, *109*, 10880−10885.
(70) Cunha, F.; Jin, Q.; Tao, N. J.; Li, C. Z. Structural phase transition in self-assembled 1,10′ phenanthroline monolayer on Au(111). *Surf. Sci.* **1997**, *389*, 19−28.
(71) Sugimasa, M.; Inukai, J.; Itaya, K. Structure of Sulfur Adlayer on Cu(111) Electrode in Alkaline Solution. *J. Electrochem. Soc.* **2003**, *150*, E110−E270.
(72) Bretti, C.; Crea, F.; De Stefano, C.; Sammartano, S. Solubility and Activity Coefficients of 2,2-Bipyridyl, 1,10-Phenanthroline and 2,2,6,2-Terpyridine in $NaCl_{(aq)}$ at Different Ionic Strengths and T = 298.15 K. *Fluid Phase Equilib.* **2008**, *272*, 47−52.
(73) Lõkov, M.; Tshepelevitsh, S.; Heering, A.; Plieger, P. G.; Vianello, R.; Leito, I. On the Basicity of Conjugated Nitrogen Heterocycles in Different Media. *Eur. J. Org. Chem.* **2017**, 4475−4489.
(74) De Robertis, A.; Foti, C.; Gianguzza, A.; Rigano, C. Protonation Thermodynamics of 1,10-Phenanthroline in Aqueous Solution. Salt Effects and Weak Complex Formation. *J. Solution Chem.* **1996**, *25*, 597−606.
(75) Ishiguro, S.-i.; Wada, H.; Ohtaki, H. Solvation and Protonation of 1,10-Phenanthroline in Aqueous Dioxane Solutions. *Bull. Chem. Soc. Jpn.* **1985**, *58*, 932−937.
(76) Mitchell, P. R. Hydrogen-1 nuclear magnetic resonance study of the self-association of 1,10-phenanthroline, 2,2′-bipyridyl, and their zinc(II) complexes. *J. Chem. Soc., Dalton Trans.* **1980**, 1079−1086.
(77) Mattsson, E.; Bockris, J. O. Galvanostatic Studies of the Kinetics of Deposition and Dissolution in the Copper + Copper Sulphate System. *Trans. Faraday Soc.* **1959**, *55*, 1586−1601.
(78) Čuljak, I.; Mlakar, M.; Branica, M. Cathodic Stripping Voltammetry of the Copper 1,10-Phenantroline Complex. *Electroanalysis* **1995**, *7*, 64−69.
(79) Quentel, F.; Madec, C. Voltammetric study of the copper-1,10-phenanthroline complex. *Anal. Chim. Acta* **1990**, *230*, 83−90.
(80) Sugiyama, K.; Aoki, K. Catalytic Reactions of Bis(1,10-Phenanthroline) Cuprous Complex with Hydrogen Peroxide at Glassy Carbon and Pyrolytic Graphite electrodes. *J. Electroanal. Chem.* **1989**, *262*, 211−219.



DOI: 10.1021/acsomega.8b02353
*ACS Omega* 2018, 3, 13636−13646